NANO LETTERS

2007
Vol. 7, No. 3
723−728

Highly Efficient Avalanche Multiphoton Luminescence from Coupled Au Nanowires in the Visible Region

Qu-Quan Wang,*,†,‡ Jun-Bo Han,† Dong-Lai Guo,† Si Xiao,† Yi-Bo Han,† Hong-Mei Gong,† and Xian-Wu Zou†

Department of Physics and Key Laboratory of Acoustic and Photonic Materials and Devices of Ministry of Education, Wuhan University, Wuhan 430072, P. R. China

Received December 16, 2006; Revised Manuscript Received February 8, 2007

ABSTRACT

We demonstrate highly efficient avalanche multiphoton luminescence (MPL) from ordered-arrayed gold nanowires (NWs) with low time-average excitation intensity, I_{exc} (5.0−9.1 kW/cm^2). The intensity of avalanche MPL, I_{MPL}, is about 10^4 times larger than that of three-photon luminescence, the slope $\partial \log I_{MPL}/\partial \log I_{exc}$ of avalanche MPL reaches as high as 18.3, and the corresponding polarization dependence of I_{MPL} has a form of $\cos^{50} \phi_p$. The emission dynamics of avalanche MPL and three-photon luminescence are also studied comparatively. These observations indicate that the highly efficient avalanche MPL is attributed to the giant enhancement and coupling of longitudinal surface plasmon resonance of ordered-arrayed gold NWs.

Surface plasmon resonance (SPR) of noble metal nanostructures has promising applications ranging from ultrafast information processing and nonlinear spectroscopy to biosensors and biolabeling.[1−5] SPR-enhanced multiphoton absorption with ultrafast laser excitation induces unexpected intensive photoemission from gold films[6,7] and efficient photoluminescence (PL) from gold nanoparticles and nanorods.[3,5,8−10]

Visible PL from gold films and nanostructures is generally assigned to the radiative recombination of excited electrons in the sp-conductive band and holes in the d-band[8,11−14] or the radiation emission of surface plasmon.[10,15] The PL intensity and the nonlinear interaction involved are strongly dependent on the nanostructure and the enhancement of local electromagnetic field. The PL from gold nanobowties induced by two-photon absorption is enhanced ∼10^3 compared to that of the smooth film.[16] A multiphoton generation process of noble metal particles was first observed in silver.[17] Farrer et al. reported three-photon-induced PL with high emission efficiency and partial emission polarization in gold nanoparticles for the first time.[8] Gold nanorods and nanowires (NWs) have two SPR absorption bands, and the peak position of longitudinal SPR is easily adjusted by controlling the aspect ratio. A stronger enhancement of local field[18,19] and smaller plasmon damping exist in gold nanorods[20] or NWs compared to nanoparticles. Wang et al. demonstrated in vivo imaging of single Au nanorods by two-photon PL.[5] Recently, visible PL involving a four-photon interaction in resonant optical antennas consisting of Au nanorods was also reported.[3] But the coupling of parallel nanorods (or NWs) is seldom reported. In this study, we demonstrate unexpected giant enhancement of visible multiphoton-induced PL (MPL) from ordered-arrayed gold NWs with strong cross relaxation, in which higher-order nonlinear processes and the avalanche effect are involved.

Our ordered-arrayed Au NWs are grown by using anodic aluminum oxide (AAO). AAO membranes are fabricated by using a two-step anodization process. The treated aluminum sheets are exposed to an H_2SO_4 acid (0.3 M) solution under a constant voltage of 19 V in an electrochemical cell at a temperature of about 4 °C for 10 h in each step. The aluminum oxide layer produced by the first anodization step is removed by wet-chemical etching in a mixture of phosphoric acid and chromic acid. Gold is deposited in the pores of AAO membranes by alternating current electrolysis (50 Hz, 9 V ac) in an electrolyte containing $HAuCl_4 \cdot 4H_2O$ (0.01 M) and H_2SO_4 acid (0.1 M) with Pt counter electrodes. Scanning electron microscopy (SEM) is performed using an FEG SEM Sirion 200 instrument operated at an accelerating voltage of 10.0 kV. Transmission electron microscopy (TEM) is performed using a JEOL2010HT instrument operated at 100 kV. The absorption spectra are recorded on a UV−vis−NIR spectrophotometer (Varian Cary500). The excitation source for MPL is a mode-locked Ti:sapphire picosecond pulsed laser (Mira 900, Coherent) with a pulse width of ∼3

* Corresponding author. E-mail: qqwang@whu.edu.cn.
† Department of Physics.
‡ Key Laboratory of Acoustic and Photonic Materials and Devices of Ministry of Education.

10.1021/nl062964f CCC: $37.00
Published on Web 02/21/2007

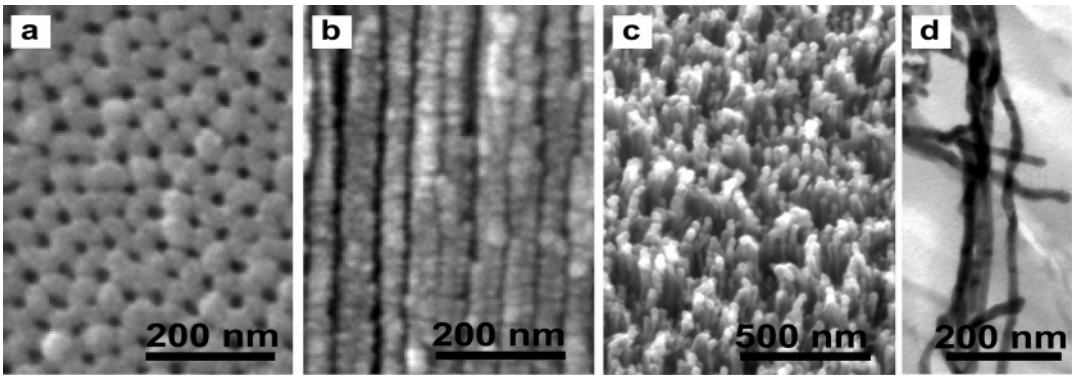

Figure 1. SEM and TEM images of Au NWs. (a) Top-view SEM image of AAO membrane. The average diameter of the arrayed holes is about ~20 nm, with separation ~25 nm. (b) Cross-section SEM image of AAO membrane. (c) SEM image of ordered-arrayed Au NWs. A thin layer of Al_2O_3 is dissolved by H_3PO_4 for the observation of NWs in the membrane. (d) TEM image of Au NWs with aspect ratio 70 (length ~1.4 μm and diameter ~20 nm).

ps and a repetition rate of 76 MHz. The visible MPL from Au NWs in the AAO membrane and the reference sample, rhodamine B (RDM-B), are recorded by spectrometry (Spectrapro 2500i, Acton) with a liquid-nitrogen-cooled CCD (SPEC-10, Princeton). The time-resolved PL decay traces are recorded by using a time-correlated single-photon-counting system (PicoQuant GmbH).

Figure 1a,b shows the top-view and cross-section SEM images of the AAO membrane. Figure 1c shows the SEM image of ordered-arrayed Au NWs. A thin layer of Al_2O_3 is dissolved by H_3PO_4 for the observation of NWs in the membrane. Figure 1d shows the TEM image of Au NWs. The aspect ratios, L/d, for Au NWs from four samples are about 23, 30, 43, and 70, respectively. From Figure 1, one can see that the ordered-arrayed Au NWs in the AAO membrane have an average diameter of ~20 nm and a separation of ~25 nm. The SP of noble metallic nanoparticles and NWs with this small separation could be coupled, and the coupling strength could increased by decreasing the separation.[3,21]

The absorption of ordered-arrayed Au NWs is strongly dependent on the incident angle and the polarization due to the separation of transverse and longitudinal SPR absorption. Figure 2a,b shows the absorption spectra of ordered-arrayed Au NWs recorded by using an unpolarized source with incident angles $\theta_{in} = 0°$ and 45°, respectively. The transverse SPR absorption was centered at ~525 nm, with a narrow band. The central peak of longitudinal SPR absorption is around 1100−1200 nm, with a broad band, which is shorter than the theoretically calculated value for a single Au NW and may be caused by the SP coupling of arrayed NWs.[21,22]

Figure 2c shows the excitation polarization dependence of the absorption of ordered-arrayed Au NWs with incident angle $\theta_{in} = 45°$ at 800 nm wavelength. The absorption (α_p) of p-polarized light ($\phi_p = 0°$) is larger than the absorption (α_s) of s-polarized light ($\phi_s = 0°$) due to the longitudinal SPR absorption, where $\phi_p = 90° - \phi_s$ is the angle between the incident plane and the polarization of the incident light. The value of α_p/α_s increases from 1.2 to 7.5 as the aspect ratio, L/d, of the NWs increases from 23 to 70. This means that the Au NWs with larger aspect ratios have larger longitudinal SPR absorptions at 800 nm wavelength. The electromagnetic field of the laser along the long axis of the NWs, $E_{||}$, is proportional to $|f_{||}(\omega) \cos \phi_p|$, where $f_{||}(\omega)$ is the corresponding field enhancement factor. So, the large α_p caused by the longitudinal SPR absorption also represents a large field enhance factor, $f_{||}(\omega)$, along the long axis of the NWs.

The MPL intensity, I_{MPL}, of ordered-arrayed Au NWs is greatly enhanced by the longitudinal SPR: a strong pink MPL is observed by using a p-polarized laser ($\lambda_{exc} = 800$ nm). The intensity of avalanche PL from Au NWs with $L/d = 70$ is 10^4 times larger than that of three-photon PL from Au NWs with $L/d = 23$, with a low time-average excitation intensity, $I_{exc} = 9.1$ kW/cm^2 (incident laser power, 100 mW; focal length of the lens, 300 mm; and focused area, ~1.1×10^3 μm^2). The optical setup for the observation of MPL is shown in Figure 3a. The inset of Figure 3a gives color photos of MPL from ordered-arrayed Au NWs with an average length of 1.4 μm ($L/d = 70$) and the reference sample RDM-B (5.7×10^{-4} M in ethanol), held in a quartz cell with thickness 1 mm, which are excited with the same intensity ($I_{exc} = 9.1$ kW/cm^2) and recorded under the same conditions. It clearly shows that the avalanche PL from ordered-arrayed Au NWs is much brighter and seems to have a much bigger area than the emission from the reference sample RDM-B in this case. Figure 3b exhibits the MPL spectra of ordered-arrayed Au NWs and the reference sample RDM-B. The center peak of MPL of ordered-arrayed Au NWs shifts from 600 to 680 nm as the aspect ratio L/d increases from 23 to 70.

The giant enhancement of MPL of Au NWs with larger aspect ratio is caused by the higher-order optical nonlinear processes and the avalanche effect. Figure 4a shows the excitation intensity dependence of visible MPL of ordered-arrayed Au NWs and the reference sample RDM-B. The PL of RDM-B is induced by two-photon absorption, and the corresponding slope, $\nu = \partial \log I_{MPL}/\partial \log I_{exc}$, is measured to be about 2.1. Much more photons are involved in the MPL of Au NWs. For the ordered-arrayed Au NWs with a relatively smaller aspect ratio, $L/d = 23$, the slope $\partial \log I_{MPL}/\partial \log I_{exc}$ is 3.1, and the MPL is induced by three-photon

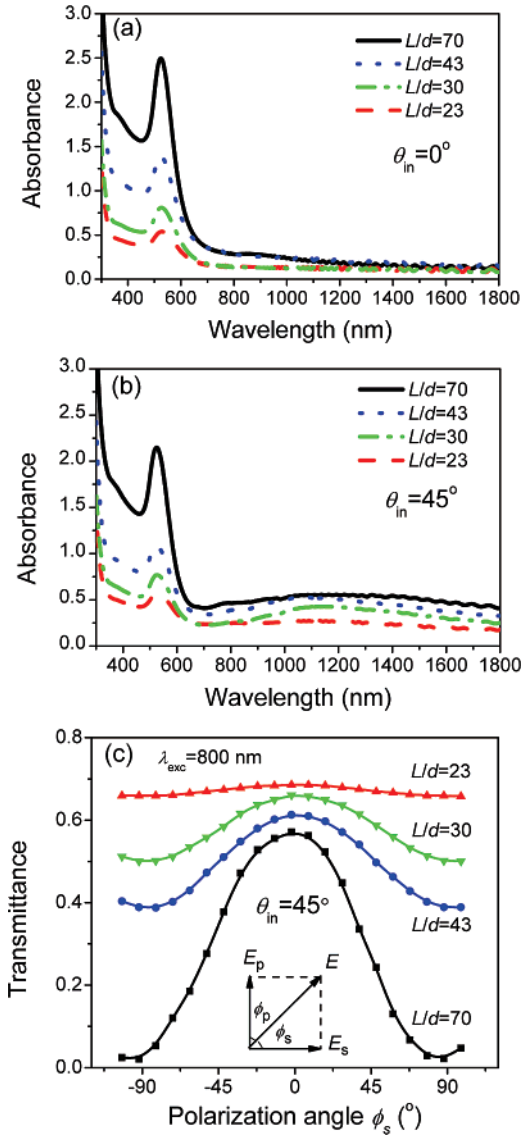

Figure 2. Absorption behaviors of the ordered-arrayed Au NWs. (a) Absorption spectra of ordered-arrayed Au NWs recoded with incident angle $\theta_{in} = 0°$. The absorption peak near 525 nm is attributed to the transverse SPR mode. (b) Absorption spectra recoded with incident angle $\theta_{in} = 45°$. The absorption peak near 1100−1200 nm is attributed to the longitudinal SPR mode. (c) The polarization dependence of the transmittance of ordered-arrayed Au NWs with incident angle $\theta_{in} = 45°$ at 800 nm wavelength. The inset illustrates the polarization angles ϕ_p and ϕ_s of the excitation laser.

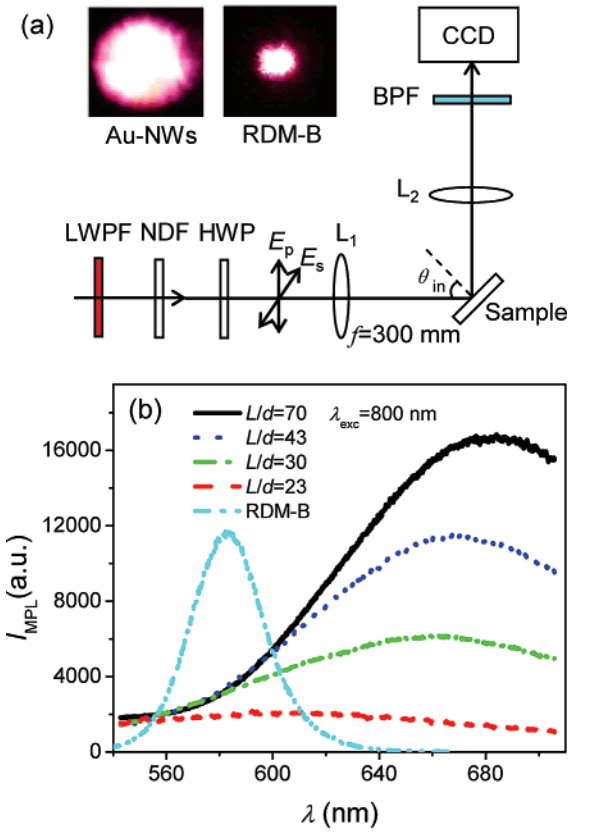

Figure 3. Visible MPL from ordered-arrayed Au NWs and reference sample RDM-B. (a) Illustration of the optical setup for excitation and recording MPL spectra. Inset shows the photos of MPL from ordered-arrayed Au NWs with thickness 1.4 μm and RDM-B (5.7×10^{-4} M in ethanol) held in a cell with thickness 1 mm ($I_{exc} = 9.1$ kW/cm^2). The excitation intensity and recoding conditions for two photos are the same. LWPF, long-wavelength pass filter; NDF, tunable neutral density filter; HWP, half-waveplate. (b) The MPL spectra of ordered-arrayed Au NWs and reference sample RDM-B.

absorption. For the ordered-arrayed Au NWs with larger aspect ratios, $L/d = 30$, 43 and 70, there are two slopes in the log I_{MPL}−log I_{exc} curves: the values of the first slope are 3.9, 5.2, and 5.6, and those of the second slope increase to as high as 14.7, 17.2, and 18.3, respectively (see Figure 4b). We believe that the first slope (in the range 3−6) represents the photons absorbed during the excitation processes; the second slope (in the range 15−18) represents avalanche PL. Both slopes increase and the threshold excitation intensity for avalanche PL decreases as the aspect ratio L/d of Au NWs increases, which is attributed to the increasing avalanche cross-relaxation rate. Avalanche PL is not observed in Au NWs with a smaller aspect ratio, $L/d = 23$, and a smaller value of the first slope, 3.1 (even if the excitation intensity increases 20 times). This means that at least four photons are involved in the avalanche PL.

The photon emission dynamics of avalanche PL is different from that of three-photon PL, as shown in Figure 5. The three-photon PL of Au NWs with $L/d = 23$ and $\nu = 3.1$ decays with a single-exponential function, and the lifetime is about 0.93 ns (see Figure 5a). This is consistent with Imura's observation in single Au nanorods,[23] but this lifetime is quite long compared to those observed in ultrafast pump−probe measurements of gold nanoparticles and nanorods.[18,20,24,25] This may be caused by the recombination of excited electrons located very close to the Fermi level with holes in the d-band.[23,26] The avalanche PL of ordered-arrayed Au NWs with $L/d = 70$ and $\nu = 18.3$ decays with a two-exponential function as

$$I_{MPL}(\tau) = A_f e^{-\tau/\tau_f} + A_s e^{-\tau/\tau_s} \quad (1)$$

where A_f and A_s are the relative intensity attributed to the fast and slow decay processes, respectively, and τ_f and τ_s are the lifetime of the corresponding processes. The value

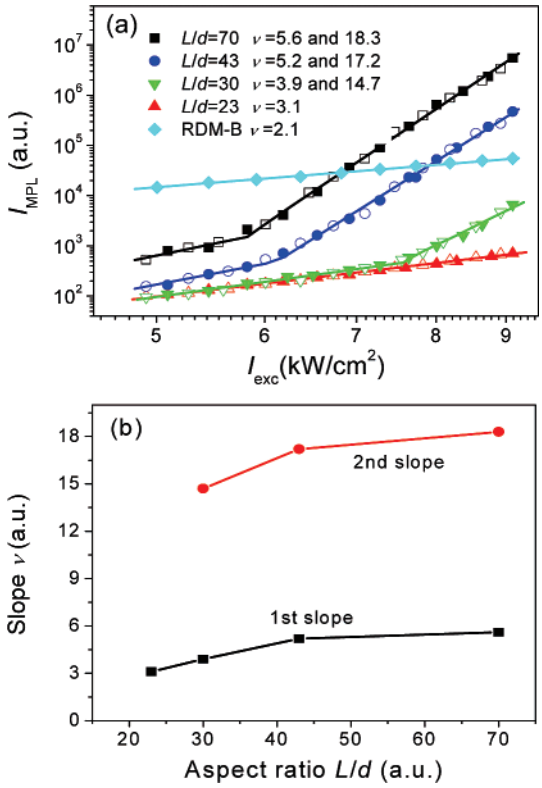

Figure 4. Excitation intensity dependence of visible MPL from ordered-arrayed Au NWs. (a) Logarithm relationship between MPL intensity, I_{MPL}, and excitation intensity, I_{exc}. The solid and the open marks are the data recorded by increasing and decreasing the excitation intensity, respectively. The slope, $\nu = \partial \log I_{MPL}/\partial \log I_{exc}$, reaches as high as 18.3 for avalanche PL from ordered-arrayed Au NWs with large aspect ratio $L/d = 70$. (b) The slope $\nu = \partial \log I_{MPL}/\partial \log I_{exc}$ versus the aspect ratio.

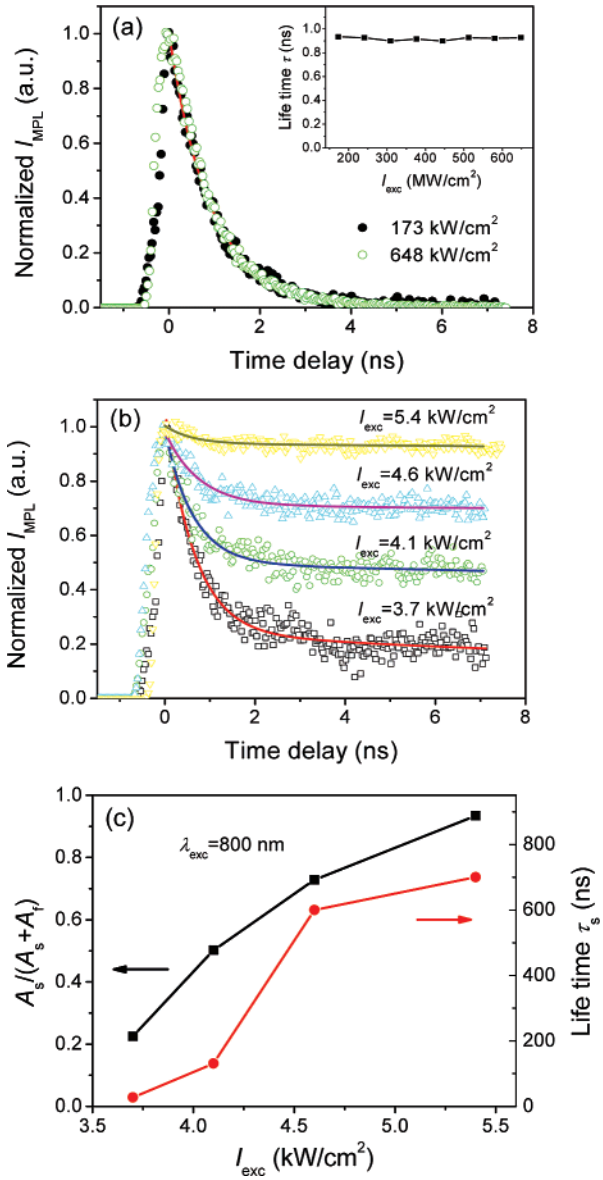

Figure 5. Emission decay traces of avalanche PL and three-photon PL from ordered-arrayed Au NWs. (a) The decay traces of three-photon PL of ordered-arrayed Au NWs ($L/d = 23$ and $\nu = 3.1$) with excitation intensity 173 and 648 kW/cm^2. The inset shows the lifetime versus excitation intensity. (b) The decay traces of avalanche PL of ordered-arrayed Au NWs ($L/d = 70$ and $\nu = 18.3$) with excitation intensity 3.7, 4.1, 4.6, and 5.4 kW/cm^2. (c) The lifetime and relative intensity of the slow decay process versus excitation intensity.

of τ_s increases from 27 to 700 ns, and $A_s/(A_f + A_s)$ increases from 0.23 to 0.93 as the excitation intensity increases from 3.7 to 5.4 kW/cm^2. The lifetime of the fast decay process is about 0.70 ± 0.05 ns and is independent of the excitation intensity. The ultraslow decay of MPL is another characteristic of the avalanche up-conversion,[27,28] which implies the existence of strong coupling and cross-relaxation in the ordered-arrayed Au NWs with larger aspect ratio and larger enhancement of longitudinal SPR, which also means that the observed avalanche PL is not caused by stimulated radiation.

The excitation wavelength dependence of the MPL of Au NWs is shown in Figure 6, which is related to the density of states as well as SPR absorption. The avalanche PL of ordered-arrayed Au NWs with larger aspect ratios of 30, 43, and 70 significantly increases as the excitation wavelength increases from 780 nm (1.59 eV) to 880 nm (1.41 eV), which is mainly caused by increasing of the SPR absorption and the corresponding increasing of the field enhancement factor. One can see that the curves of MPL excitation (PLE) coincide with the absorption spectra very well. But the three-photon PL of the Au NWs with a relatively small aspect ratio of 23 decreases as the excitation wavelength increases from 780 to 880 nm, which is caused by the relatively large density of states of Au nanomaterials near 4.9 eV (~250 nm).[9,14] The electrons are excited to this high-level region with a large density of states by absorption of three photons with a wavelength of 780 nm (1.59 eV), which leads to a larger intensity of three-photon PL at the shorter wavelength (780 nm) shown in Figure 6.

The avalanche PL intensity of ordered-arrayed Au NWs is very sensitive to the polarization of the excitation field due to a large field enhancement factor along the long axis of the Au NWs and a large slope, $\nu = \partial \log I_{MPL}/\partial \log I_{exc}$. Figure 7 shows the excitation polarization dependence of avalanche PL from ordered-arrayed Au NWs with $L/d = 70$ and $\nu = 18.3$, which is well fitted by $\cos^{50} \phi_p$. For comparison, the excitation polarization dependence of three-photon PL from ordered-arrayed Au NWs with $L/d = 23$ and $\nu = 3.1$ is also shown in Figure 7; it has approximately

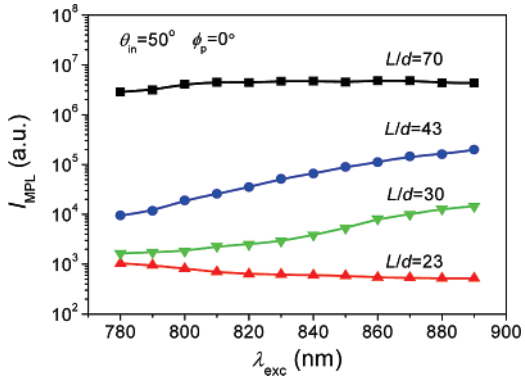

Figure 6. Excitation wavelength dependence of avalanche PL and three-photon PL of ordered-arrayed Au NWs. (a) As the excitation wavelength increases from 780 nm (1.59 eV) to 890 nm (1.39 eV), the avalanche PL of ordered-arrayed Au NWs with larger aspect ratios of 30, 43, and 70 significantly increases due to the increasing field enhancement factor, while the three-photon PL of Au NWs with a relatively small aspect ratio of 23 decreases due to the larger density of states of Au nanomaterials at a high energy level, near 4.9 eV.

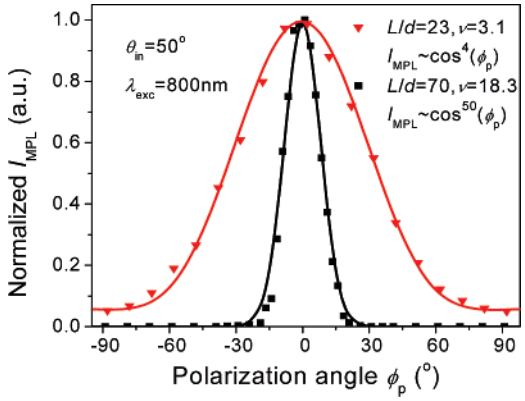

Figure 7. Excitation polarization dependence of avalanche PL and three-photon PL of ordered-arrayed Au NWs. The excitation polarization dependence of avalanche PL from ordered-arrayed Au NWs with $L/d = 70$ and $\nu = 18.3$ is fitted by $\cos^{50} \phi_p$. That of three-photon PL from ordered-arrayed Au NWs with $L/d = 23$ and $\nu = 3.1$ has approximately the form $a + b \cos^4 \phi_p$.

the form of $a + b \cos^4 \phi_p$. The excitation polarization dependence of MPL of a coupled Au NWs array is also dependent on the excitation intensity and incident angle, in contrast to single Au nanorods.

The MPL of ordered-arrayed Au NWs in an AAO membrane has much better photostability than that of the Au nanorods prepared by electron-beam lithography or seeded growth in micelles.[5,10,29] The AAO membrane, with good mechanical and electronic isolating properties, controls the shape and confines the excited electron of the Au NWs. The intensity of MPL does not significantly change after hours of measurements. The slope $\partial \log I_{MPL}/\partial \log I_{exc}$, measured by increasing and decreasing the excitation intensity, has the same values within the measurement error (see Figure 4a). Another reason for the better photostability is the low time-average excitation intensity, ~10 kW/cm^2, and the low peak excitation intensity, ~40 MW/cm^2, used in our measurements. The optical nonlinear effects, such as nonlinear absorption and nonlinear refraction (NLR), are enhanced with increasing excitation intensity and SPR absorption at the excitation frequency. The NLR effect in the ordered-arrayed Au NWs is not observed in the close-aperture *Z*-scan measurements at this low excitation intensity region, even though the SPR absorption at 800 nm is strong,[30,31] which excludes the contribution of self-focus effect caused by positive NLR to the high-order nonlinear MPL of Au NWs.

PL from gold in the visible region is generally assigned to the radiative interband transition of an electron−hole pair[8,11−14] or SPR emission.[10,15] The former is more convincing to explain our observed visible MPL centered around 600−680 nm, since the transverse and longitudinal SPR absorption peaks are around 525 and 1100 nm, respectively. The observed visible PL is mainly attributed to the recombination of sp-electrons near the Fermi level and the d-holes near the *X* symmetry point.[23] The strong MPL is attributed to the great enhancement of incoming (excitation) and outgoing (emission) field. During the excitation processes, the probability of *m*-fold excited electrons is proportional to $|f(\omega_{exc})|^{2m}$ ($m \geq 2$), where $f(\omega_{exc})$ is the field enhancement factor at the excitation frequency and *m* represents the order of the optical nonlinear interaction. The photoemissions induced by multiphoton absorption and multiple excitation of surface plasmon are observed in gold films[6,32] and silver nanoparticles.[33] The strong field enhancement greatly increases the probability to excite the electrons to higher levels by multiphoton absorption and multiple excitation of surface plasmon. So, we think that the interplay of multiphoton absorption and/or multiple excitation of surface plasmon and coupling of longitudinal SPR lead to the unexpectedly strong visible MPL of ordered-arrayed Au NWs with unexpectedly large slope, $\partial \log I_{MPL}/\partial \log I_{exc}$. But the details of the nonlinear interaction, the cross-relaxation processes, and the mechanism of avalanche PL need to be further studied. We believe these observations have promising applications in up-conversion, sensors, and optical information processing.

Acknowledgment. Thank to Z. K. Zhou and M. Li for their assistance in PL measurement. This work was supported by NSFC (Grants 10534030 and 10474075), National Program on Key Science Research (2006CB921500), and Program for NCET.

References

(1) Hu, M. S.; Chen, H. L.; Shen, C. H.; Hong, L. S.; Huang, B. R.; Chen, K. H.; Chen, L. C. *Nature Mater.* **2006**, *5*, 102.
(2) Pardo-Yissar, V.; Gabai, R.; Shipway, A. N.; Bourenko, T.; Willner, I. *Adv. Mater.* **2001**, *13*, 1320.
(3) Mühlschlegel, P.; Eisler, H.-J.; Martin, O. J. F.; Hecht, B.; Pohl, D. W. *Science* **2005**, *308*, 1607.
(4) Imura, K.; Nagahara, T.; Okamoto, H. *J. Am. Chem. Soc.* **2004**, *126*, 12730.
(5) Wang, H. F.; Huff, T. B.; Zweifel, D. A.; He, W.; Low, P. S.; Wei, A.; Cheng, J. X. *Proc. Natl. Acad. Sci. U.S.A.* **2005**, *102*, 15752.
(6) Farkas, G.; Tóth, C.; Köházi-Kis, A.; Agostini, P.; Martin, P.; Berset, J. M.; Ortega, J. M. *J. Phys. B* **1998**, *31*, L461.
(7) Kupersztych, J.; Raynaud, M. *Phys. Rev. Lett.* **2005**, *95*, 147401.
(8) Farrer, R. A.; Butterfield, F. L.; Chen, V. W.; Fourkas, J. T. *Nano Lett.* **2005**, *5*, 1139.
(9) Wilcoxon, J. P.; Martin, J. E. *J. Chem. Phys.* **1998**, *108*, 9137.
(10) Bouhelier, A.; Bachelot, R.; Lerondel, G.; Kostcheev, S.; Royer, P.; Wiederrecht, G. P. *Phys. Rev. Lett.* **2005**, *95*, 267405.

(11) Mooradian, A. *Phys. Rev. Lett.* **1969**, *22*, 185.
(12) Boyd, G. T.; Yu, Z. H.; Shen, Y. R. *Phys. Rev. B* **1986**, *33*, 7923.
(13) Beversluis, M. R.; Bouhelier, A.; Novotny, L. *Phys. Rev. B* **2003**, *68*, 115433.
(14) Lin, H. Y.; Chen, Y. F. *Appl. Phys. Lett.* **2006**, *88*, 101914.
(15) Dulkeith, E.; Niedereichholz, T.; Klar, T. A.; Feldmann, J. *Phys. Rev. B* **2004**, *70*, 205424.
(16) Schuck, P. J.; Fromm, D. P.; Sundaramurthy, A.; Kino, G. S.; Moerner, W. E. *Phys. Rev. Lett.* **2005**, *94*, 017402.
(17) Monti, O. L. A.; Fourkas, J. T.; Nesbitt, D. J. *J. Phys. Chem. B* **2004**, *108*, 1604.
(18) Varnavski, O. P.; Mohamed, M. B.; El-Sayed, M. A.; Goodson, T., III. *J. Phys. Chem. B* **2003**, *107*, 3101.
(19) Mohamed, M. B.; Volkov, V.; Link, S.; El-Sayed, M. A. *Chem. Phys. Lett.* **2000**, *317*, 517.
(20) Sönnichsen, C.; Franzl, T.; Wilk, T.; von Plessen, G.; Feldmann, J. *Phys. Rev. Lett.* **2002**, *88*, 077402.
(21) Jain, P. K.; Eustis, S.; El-Sayed, M. A. *J. Phys. Chem. B* **2006**, *110*, 18243.
(22) Link, S.; Mohamed, M. B.; El-Sayed, M. A. *J. Phys. Chem. B* **1999**, *103*, 3073.
(23) Imura, K.; Nagahara, T.; Okamoto, H. *J. Phys. Chem. B* **2005**, *109*, 13214.
(24) Sun, C.-K.; Vallée, F.; Acioli, L. H.; Ippen, E. P.; Fujimoto, J. G. *Phys. Rev. B* **1994**, *50*, 15337.
(25) Varnavski, O. P.; Goodson, T., III; Mohamed, M. B.; El-Sayed, M. A. *Phys. Rev. B* **2005**, *72*, 235405.
(26) Kittel, C. *Introduction to Solid State Physics*; John Wiley & Sons: New York, 1986.
(27) Lahoz, F.; Martín, I. R.; Guadalupe, V. L.; Méndez-Ramos, J.; Rodríguez, V. D.; Rodríguez-Mendoza, U. R. *Opt. Mater.* **2004**, *25*, 209.
(28) Shu, Q.; Rand, S. C. *Phys. Rev. B* **1997**, *55*, 8776.
(29) Link, S.; Burda, C.; Nikoobakht, B.; El-Sayed, M. A. *J. Phys. Chem. B* **2000**, *104*, 6152.
(30) Sheik-Bahae, M.; Said, A. A.; Wei, T. H.; Hagan, D. J.; Van Stryland, E. W. *IEEE J. Quantum Electron.* **1990**, *26*, 760.
(31) Wang, Q. Q.; Han, J. B.; Gong, H. M.; Chen, D. J.; Zhao, X. J.; Feng, J. Y.; Ren, J. J. *Adv. Funct. Mater.* **2006**, *16*, 2405.
(32) Georges, A. T. *Phys. Rev. A* **2002**, *66*, 063412.
(33) Merschdorf, M.; Pfeiffer, W.; Thon, A.; Voll, S.; Gerber, G. *Appl. Phys. A* **2000**, *71*, 547.

NL062964F